A novel immersed boundary method for the strongly coupled fluid-structure interaction

*,†**Shang-Gui Cai**[1] **and Abdellatif Ouahsine**[1]

[1]Sorbonne Universités, Université de Technologie de Compiègne, CNRS, UMR 7337 Roberval, Centre de Recherche Royallieu, CS 60319, 60203 Compiègne Cedex, France

*Presenting author: shanggui.cai@utc.fr

†Corresponding author: shanggui.cai@utc.fr

ABSTRACT

In the present work a novel non-body conforming mesh method, termed as the moving immersed boundary method, is proposed for the strongly coupled fluid-structure interaction. The immersed boundary method enables solids of complex shape to move arbitrarily in an incompressible viscous fluid, without fitting the solid boundary motion with dynamic meshes. A boundary force is usually employed to impose the no-slip boundary condition at the solid surface. In the novel method, an additional equation is derived to compute the boundary force implicitly. The coefficient matrix is formulated to be symmetric and positive-definite, so that the conjugate gradient method can solve the resulting system very efficiently. The current immersed boundary solver is integrated into the fluid projection method as another operator splitting. Finally an efficient fixed point iteration scheme is constructed for the strongly coupled fluid-structure interaction.

Keywords: Immersed boundary method, Fluid-structure interaction, Strongly coupled algorithm, Projection method, Fractional step method.

Introduction

The fluid-structure interaction (FSI) is of great importance in many scientific and engineering fields. The difficulties of its numerical simulation lie in the facts that the interaction interface is often complicated, time-dependent and the two physical domains are strongly coupled. The FSI problem has been extensively studied in the past with body-conforming mesh methods, such as the arbitrary Lagrangian-Eulerian (ALE) method, where the mesh is deformed or renewed in order to fit the novel interface (e.g. [1]). This procedure however is usually time-consuming and it is very difficult to maintain the mesh quality when solids undergo large displacements.

The immersed boundary method (IBM) emerged in 1970s by the work of Peskin [8] as an effective tool to circumvent the dynamic mesh issues. A boundary force is introduced to the fluid momentum equation to account for the solid effects, hence the fluid equations are solved on a fixed Eulerian grid. The original method is developed for the simulation of blood flow over an elastic beating heart. Its direct extension to rigid boundary poses a lot of difficulties, since the stiffness value approaches infinity. The time step is also kept very small in order to maintain the stability. This method has been successfully extended to moving rigid bodies by the work of Uhlmann [9] by using the direct forcing concept of [3]. No artificial constants and additional time constraint are introduced for the rigid body formulation. However, fully explicit schemes were adopted for the force evaluation and the interface coupling in [9]. Consequently, the no-slip boundary condition is never satisfied and the calculation will not be stable when the solid density is smaller or even close to the fluid density ($\rho_s/\rho_f \lesssim 1.05$ for

circular disks as reported in [9]).

Therefore, implicit schemes should be considered for obtaining accurate and stable results. In this work we extend the implicit immersed boundary method of [2] to two-way fluid-structure interactions in the next section. We will demonstrate the stability and the accuracy of present scheme in the numerical examples.

Numerical method

Governing equations

In the present study, we consider the rigid body motion in an incompressible fluid. The fluid-structure interaction problem is illustrated in Figure 1, where the fluid and the rigid body occupy the domain Ω_f and Ω_s respectively. The interaction takes place at the their common boundary $\partial\Omega_i = \Omega_f \cap \Omega_s$. The whole system is subjected to the gravitational acceleration $\mathbf{g}$.

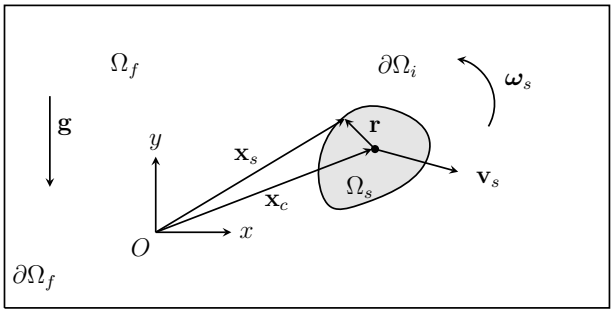

Figure 1: Sketch of the fluid-structure interaction problem.

The fluid motion is governed by the Navier-Stokes equations

$$\frac{\partial \mathbf{v}_f}{\partial t} + \nabla \cdot (\mathbf{v}_f \otimes \mathbf{v}_f) = \nabla \cdot \boldsymbol{\sigma}_f + \mathbf{g} \tag{1a}$$

$$\nabla \cdot \mathbf{v}_f = 0 \tag{1b}$$

where $\mathbf{v}_f$ is the fluid velocity vector and the fluid stress tensor $\boldsymbol{\sigma}_f$ is given by

$$\boldsymbol{\sigma}_f = -\frac{p}{\rho_f}\mathbf{I} + \nu(\nabla \mathbf{v}_f + (\nabla \mathbf{v}_f)^{\mathrm{T}}) \tag{1c}$$

where p is the fluid pressure, ρ_f the fluid density, ν the fluid kinematic viscosity. Appropriate initial and boundary conditions are assumed to the fluid Navier-Stokes equations to ensure that the problem is well posed.

The rigid body motion is governed by the Newton-Euler equations

$$m_s \frac{d\mathbf{v}_s}{dt} = \rho_f \int_{\partial\Omega_i} \boldsymbol{\sigma}_f \cdot \mathbf{n} ds + m_s(1 - \frac{\rho_f}{\rho_s})\mathbf{g} \tag{2a}$$

$$I_s \frac{d\boldsymbol{\omega}_s}{dt} = \rho_f \int_{\partial\Omega_i} \mathbf{r} \times \left(\boldsymbol{\sigma}_f \cdot \mathbf{n}\right) ds \tag{2b}$$

where m_s, ρ_s, I_s represent the solid mass, the solid density and the moment of inertia respectively. $\mathbf{v}_s$, $\boldsymbol{\omega}_s$ designate the translational velocity and the angular velocity of the solid. $\mathbf{r} = \mathbf{x}_s - \mathbf{x}_c$ is the position

vector of the surface point with respect to the solid mass center, where $\mathbf{x}_s$ is the solid position vector at the surface and $\mathbf{x}_c$ is the solid gravity center vector (see Figure 1). $\mathbf{n}$ represents the outward-pointing normal vector to the surface $\partial\Omega_i$. The position of the rigid body can be obtained by the integration of the following kinematic equations

$$\frac{d\mathbf{x}_c}{dt} = \mathbf{v}_s \tag{3a}$$

$$\frac{d\boldsymbol{\theta}_c}{dt} = \boldsymbol{\omega}_s \tag{3b}$$

where $\boldsymbol{\theta}_c$ designates the rotation angle around the solid mass center.

On the fluid-structure interface $\partial\Omega_i$ the following no-slip boundary condition

$$\mathbf{v}_f = \mathbf{v}_s + \boldsymbol{\omega}_s \times \mathbf{r} \tag{4}$$

needs to be satisfied in order to take the fluid-structure interaction into account.

The immersed boundary method approximates the above fluid-structure interaction problem by replacing the solid domain with the surrounding fluid. To account for the presence of the immersed solid, a boundary force $\mathbf{f}$ is introduced and added into the fluid momentum equation. Therefore the fluid is simply simulated in a fixed domain $\overline{\Omega} = \Omega_f(t) \cup \Omega_s(t)$ irrespective to the movement of the immersed solid. Following Glowinski *et al.* [4], we write the entire fluid-structure interaction problem in the immersed boundary formulation as

$$\frac{\partial \mathbf{v}_f}{\partial t} + \nabla \cdot (\mathbf{v}_f \otimes \mathbf{v}_f) = -\frac{1}{\rho_f}\nabla p + \nu \nabla^2 \mathbf{v}_f + \mathbf{f} \quad \text{in } \overline{\Omega} \tag{5a}$$

$$\nabla \cdot \mathbf{v}_f = 0 \quad \text{in } \overline{\Omega} \tag{5b}$$

$$\mathbf{v}_f = \mathbf{v}_s + \boldsymbol{\omega}_s \times \mathbf{r} \quad \text{on } \partial\Omega_i \tag{5c}$$

$$m_s \frac{d\mathbf{v}_s}{dt} = -\rho_f \int_{\Omega_s} \mathbf{f} dV + m_s(1 - \frac{\rho_f}{\rho_s})\mathbf{g} \tag{5d}$$

$$I_s \frac{d\boldsymbol{\omega}_s}{dt} = -\rho_f \int_{\Omega_s} \mathbf{r} \times \mathbf{f} dV \tag{5e}$$

$$\frac{d\mathbf{x}_c}{dt} = \mathbf{v}_s \tag{5f}$$

$$\frac{d\boldsymbol{\theta}_c}{dt} = \boldsymbol{\omega}_s \tag{5g}$$

where the effect of gravity in the fluid momentum equation is from now on incorporated into the pressure.

Moving immersed boundary method for strongly coupled FSI

We first discretize the governing equations as

$$\frac{{\mathbf{v}_f}^{n+1} - {\mathbf{v}_f}^{n}}{\Delta t} + \frac{3}{2}\mathcal{N}({\mathbf{v}_f}^{n}) - \frac{1}{2}\mathcal{N}({\mathbf{v}_f}^{n-1}) = -\frac{1}{\rho_f}\mathcal{G}p^{n+1} + \frac{\nu}{2}\mathcal{L}({\mathbf{v}_f}^{n+1} + {\mathbf{v}_f}^{n}) + \mathcal{S}\mathbf{F}^{n+1} \tag{6a}$$

$$\mathcal{D}{\mathbf{v}_f}^{n+1} = 0 \tag{6b}$$

$$\mathcal{T}{\mathbf{v}_f}^{n+1} = {\mathbf{v}_s}^{n+1} + {\boldsymbol{\omega}_s}^{n+1} \times \mathbf{r}^{n+1} \tag{6c}$$

$$m_s \frac{{\mathbf{v}_s}^{n+1} - {\mathbf{v}_s}^{n}}{\Delta t} = -\rho_f \mathbf{F}^{n+1} + m_s(1 - \frac{\rho_f}{\rho_s})\mathbf{g} \tag{6d}$$

$$I_s \frac{{\boldsymbol{\omega}_s}^{n+1} - {\boldsymbol{\omega}_s}^{n}}{\Delta t} = -\rho_f \mathbf{r} \times \mathbf{F}^{n+1} \tag{6e}$$

$$\frac{{\mathbf{x}_c}^{n+1} - {\mathbf{x}_c}^{n}}{\Delta t} = {\mathbf{v}_s}^{n+1} \tag{6f}$$

$$\frac{{\boldsymbol{\theta}_c}^{n+1} - {\boldsymbol{\theta}_c}^{n}}{\Delta t} = {\boldsymbol{\omega}_s}^{n+1} \tag{6g}$$

where $\mathcal{L}$, $\mathcal{N}$, $\mathcal{D}$, $\mathcal{G}$ are the discrete Laplacian, convective, divergence, gradient operators respectively. Since the fluid mesh in general does not coincident with the solid mesh, $\mathcal{T}$ and $\mathcal{S}$ are the interpolation and spreading operators to exchange the flow quantities on both meshes, which can be constructed from the discrete delta functions as in [8]. $\mathbf{F}$ designates the boundary force defined on the solid surface and thus we have $\mathbf{f} = \mathcal{S}\mathbf{F}$. $n+1$ represents the time level to be solved. Here the convection is treated explicitly with a second order Adams-Bashforth scheme but the diffusion is handled implicitly with a second order Crank-Nicolson scheme. Hence the overall scheme is stable under the standard CFL condition.

To solve above coupled fluid-structure system, we perform the following fractional step scheme:

(1) Prediction step for ${\hat{\mathbf{v}}_f}^{n+1}$

$$\frac{{\hat{\mathbf{v}}_f}^{n+1} - {\mathbf{v}_f}^{n}}{\Delta t} + \frac{3}{2}\mathcal{N}({\mathbf{v}_f}^{n}) - \frac{1}{2}\mathcal{N}({\mathbf{v}_f}^{n-1}) = -\frac{1}{\rho_f}\mathcal{G}p^n + \frac{\nu}{2}\mathcal{L}({\hat{\mathbf{v}}_f}^{n+1} + {\mathbf{v}_f}^{n}) \tag{7}$$

(2) Immersed boundary forcing step for the interface coupling

$$\frac{{\tilde{\mathbf{v}}_f}^{n+1} - {\hat{\mathbf{v}}_f}^{n+1}}{\Delta t} = \mathcal{S}\mathbf{F}^{n+1} \tag{8a}$$

$$\mathcal{T}{\tilde{\mathbf{v}}_f}^{n+1} = {\mathbf{v}_s}^{n+1} + {\boldsymbol{\omega}_s}^{n+1} \times \mathbf{r}^{n+1} \tag{8b}$$

Applying (8b) to (8a), we obtain

$$\mathcal{M}\mathbf{F}^{n+1} = \frac{{\mathbf{v}_s}^{n+1} + {\boldsymbol{\omega}_s}^{n+1} \times \mathbf{r}^{n+1} - \mathcal{T}{\hat{\mathbf{v}}_f}^{n+1}}{\Delta t} \tag{9a}$$

$${\tilde{\mathbf{v}}_f}^{n+1} = {\hat{\mathbf{v}}_f}^{n+1} + \Delta t \mathcal{S}\mathbf{F}^{n+1} \tag{9b}$$

where $\mathcal{M}$ is termed as the moving force matrix ($\mathcal{M} = \mathcal{T}\mathcal{S}$) in [2], which is found to be symmetric and positive-definite.

For the interface coupling, the solid velocity and position are solved with this moving force equation through a fixed point iteration, namely iterating (6d)-(6e)-(6f)-(6g)-(9a) until convergence. At each subiteration, the moving force equation is solved with the conjugate gradient method.

(3) Projection step for obtaining a divergence free velocity ${\mathbf{v}_f}^{n+1}$

$$\frac{{\mathbf{v}_f}^{n+1} - {\tilde{\mathbf{v}}_f}^{n+1}}{\Delta t} = -\mathcal{G}\phi^{n+1} \tag{10a}$$

$$\mathcal{D}{\mathbf{v}_f}^{n+1} = 0 \tag{10b}$$

where ϕ is the pseudo pressure. Applying the divergence operator to (10a) along with the divergence free condition (10a) gives

$$\mathcal{L}\phi^{n+1} = \frac{1}{\Delta t}\mathcal{D}{\tilde{\mathbf{v}}_f}^{n+1} \tag{11a}$$

$$\mathbf{v}_f{}^{n+1} = \tilde{\mathbf{v}}_f{}^{n+1} - \Delta t \mathcal{G}\phi^{n+1} \tag{11b}$$

The final pressure is advanced by

$$p^{n+1} = p^n + \phi^{n+1} - \frac{\nu}{2}\mathcal{D}\hat{\mathbf{v}}_f{}^{n+1} \tag{12}$$

where the last term is the splitting error resulted from velocity prediction and now is absorbed into the pressure. This type of projection method yields a consistent pressure boundary condition and thus free of numerical boundary layer, termed as the rotational incremental pressure correction projection method in [5].

The novel strongly coupled scheme is computational inexpensive, since the time-consuming pressure Poisson equation is not evolved in the interface coupling and the moving force equation is very easy to solve. We will demonstrate the novel scheme in the following numerical examples.

Results

Freely falling and rising cylinder in an infinite quiescent fluid

We first consider a circular cylinder freely falling and rising in an infinite quiescent fluid. This phenomenon happens frequently in nature and a large amount of work can be found in the literature. Here we compare our numerical results with the data of [6][7]. Namkoong *et al.* [7] performed the simulation using a body-fitted ALE formulation while Lacis *et al.* [6] employed the immersed boundary projection method.

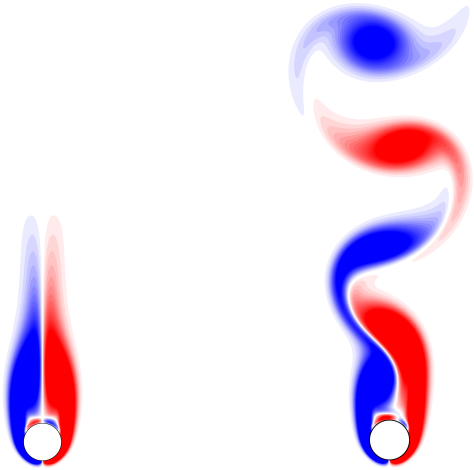

Figure 2: Vorticity fields for a freely falling cylinder in an open domain: (Left) $tV_t/D = 10$ and (right) $tV_t/D = 90$. The contour level is set from -6 (blue) to 6 (red) with an increment of 0.4.

Two density ratios are considered in this study, i.e. $\rho_s/\rho_f = 1.01$ for the falling case and $\rho_s/\rho_f = 0.99$ for the rising simulation. A large computational domain is taken as $[-5D, 5D] \times [-70D, 70D]$ with free-slip boundary conditions applied at all exterior boundaries, where $D = 0.5$ cm is the cylinder diameter. A uniform mesh is employed to cover the computational domain, and the mesh resolution is kept to $0.04D$ in order to compare with Lacis *et al.* [6]. Initially the cylinder is located at $\pm 65D$, depending on the situation ($65D$ for the falling case, $-65D$ for the rising case). The Reynolds number

$Re = V_t D/\nu_f$ is 156, where V_t is the terminal velocity. Note that the Reynolds number depends on the Galileo number $G = (|\rho_s/\rho_f - 1|gD^3)^{1/2}/\nu_f$ (here $G = 138$) and the density ratio ρ_s/ρ_f.

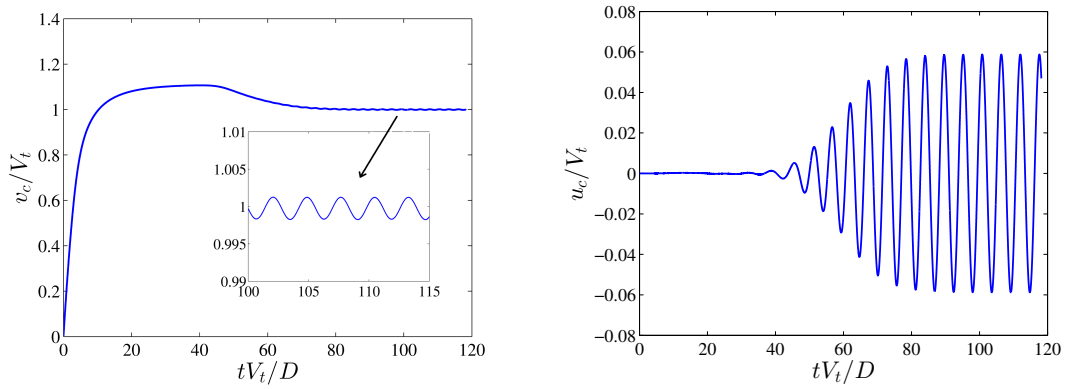

Figure 3: Time histories of the vertical and horizontal velocity for the freely rising cylinder $\rho_s/\rho_f = 0.99$.

Table 1: The drag, lift coefficients and the Strouhal number for the freely falling and rising circular cylinder in an open domain.

		C_D	max$\|C_L\|$	St
$\rho_s/\rho_f = 1.01$	Present	1.35	0.10	0.189
	Lacis *et al.* [6]	1.29	0.14	0.17185
	Namkoong *et al.* [7]	1.23	0.15	0.1684
$\rho_s/\rho_f = 0.99$	Present	1.35	0.10	0.189
	Lacis *et al.* [6]	1.29	0.14	0.17188
	Namkoong *et al.* [7]	-	-	0.1687

The vorticity fields are presented in Figure 2 for the falling cylinder case. Initially symmetric vortex pair forms behind the cylinder in the beginning of falling. After that the numerical error accumulates and breaks the symmetry. At around $tV_t/D = 40$, the flow becomes unsteady and periodic vortex shedding occurs. The time histories of the velocity components of the cylinder are plotted in Figure 3. Table 1 shows the Strouhal number $St = fD/V_t$ (f is the shedding frequency) and the coefficients of drag and lift. Present results are compared to those of [6][7]. Good agreements have been obtained.

Elliptical particle sedimentation in a confined channel

Next we consider the sedimentation of an elliptical particle in a narrow channel, to demonstrate the ability of current FSI algorithm for handling non-circular object. This example was studied previously by Xia *et al.* [10] for the boundary effects on the sedimentation mode. In their work, a multi-block lattice Boltzmann method is used and compared to the traditional ALE formulation.

To compare with Xia *et al.* [10], the computational domain is selected to be $[0, L] \times [0, 7L]$ with $L = 0.4$ cm. The aspect ratio of the ellipse is $\alpha = a/b = 2$, where a and b are the major and minor

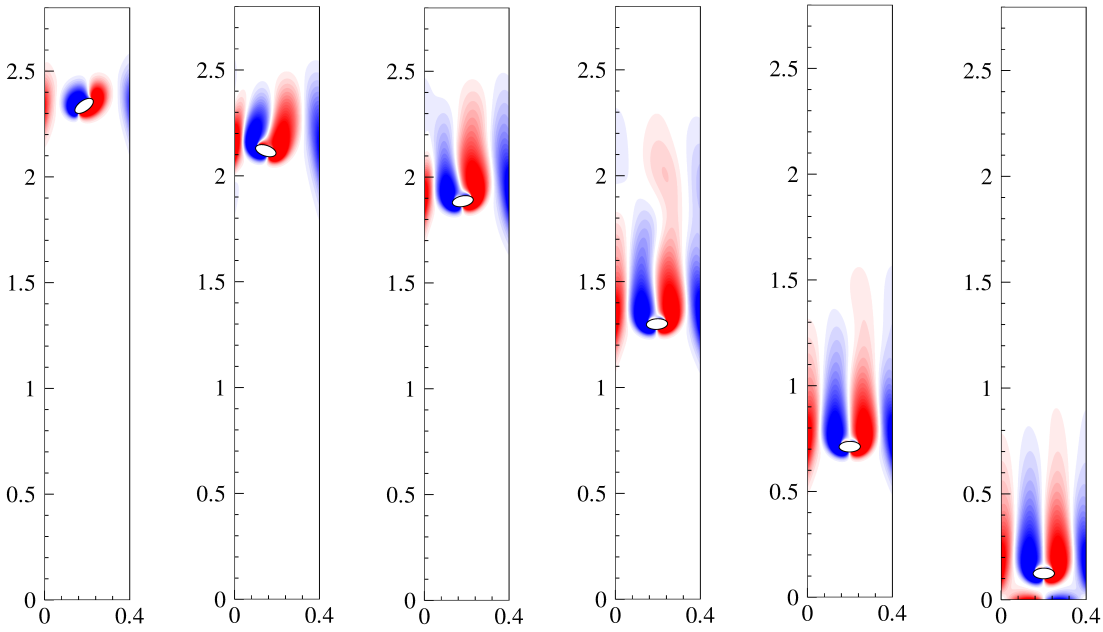

Figure 4: Vorticity fields at different times: (from left to right) t = 0.1 s, 0.3 s, 0.5 s, 1.0 s, 1.5 s, 2.0 s. The contour levels are set from -15 (blue) to 15 (red).

axes respectively. The blockage ratio is defined as $\beta = L/a = 4$. The density ratio is $\rho_s/\rho_f = 1.1$. The kinematic viscosity of fluid is set to $\nu = 0.01$ cm^2/s. The particle starts falling in a quiescent fluid from the centroid at $(0.5L, 6L)$ with an initial angle of $\pi/4$ to break the symmetry.

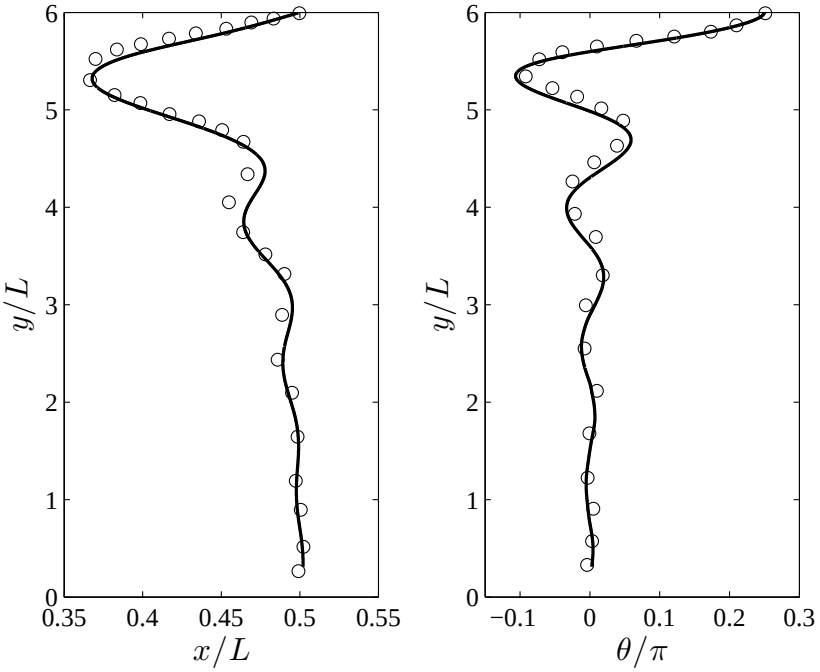

Figure 5: Particle trajectory and orientation of the elliptical particle. ”—”, present results; ”∘”, results of [10].

No-slip boundary conditions are applied at four boundaries. A uniform mesh is employed with a gird resolution of 0.0027 cm. The time step is chosen such that the CFL condition is satisfied. Figure 4 shows the vorticity fields at different times at $t = 0.1$ s, 0.3 s, 0.5 s, 1.0 s, 1.5 s, 2.0 s. The trajectory and orientations are compared to the results of [10] in Figure 5. Good agreements have been obtained.

Conclusions

In this work an efficient strongly coupled fluid-structure interaction scheme was proposed in the context of the moving immersed boundary method. To accurately impose the no-slip boundary condition at the immersed interface, a moving force equation was derived and solved with the conjugate gradient method. The global scheme follows a fractional step manner while the interface coupling was accomplished between the solid motion equations with the moving force equation in the immersed boundary forcing step. Stable results were obtained even when the solid density is smaller than the fluid density. Numerical results have demonstrated the accuracy of the proposed method.

Acknowledgements

The support of the China Scholarship Council is greatly acknowledged.

References

[1] Cai, S.-G., Ouahsine, A. and Sergent, P. (2016) Modelling wave energy conversion of a semi-submerged heaving cylinder. *In Ibrahimbegovic, A. editor, Computational Methods for Solids and Fluids: Multiscale Analysis, Probability Aspects, Model Reduction and Software Coupling*, 67–79.

[2] Cai, S.-G., Ouahsine, A., Favier, J. and Hoarau, Y. (2016) Improved implicit immersed boundary method via operator splitting. *In Ibrahimbegovic, A. editor, Computational Methods for Solids and Fluids: Multiscale Analysis, Probability Aspects, Model Reduction and Software Coupling*, 49–66.

[3] Fadlun, E.A., Verzicco, R., Orlandi, P., and Mohd-Yusof, J. (2000) Combined immersed boundary finite-difference methods for three-dimensional complex flow simulations. *Journal of Computational Physics* **161**, 35–60.

[4] Glowinski, R., Pan, T.W., Hesla, T.I., Joseph, D.D., and Périaux, J. (2001) A fictitious domain approach to the direct numerical simulation of incompressible viscous flow past moving rigid bodies: application to particulate flow. *Journal of Computational Physics* **169**, 363–426.

[5] Guermond, J.L., Minev, P., and Shen, J. (2006) An overview of projection methods for incompressible flows. *Computer Methods in Applied Mechanics and Engineering* **195**, 6011–6045.

[6] Lacis, U., Taira K. and Bagheri, S. (2016): A stable fluid-structure-interaction solver for low-density rigid bodies using the immersed boundary projection method. *Journal of Computational Physics* **305**, 300–318.

[7] Namkoong, K., Yoo, J.Y., and Choi, H.G. (2008) Numerical analysis of two-dimensional motion of a freely falling circular cylinder in an infinite fluid. *Journal of Fluid Mechanics* **604**, 33–53.

[8] Peskin, C.S. (1972) Flow patterns around heart valves: A numerical method. *Journal of Computational Physics* **10**, 252–271.

[9] Uhlmann, M. (2005) An immersed boundary method with direct forcing for the simulation of particulate flows. *Journal of Computational Physics* **209**, 448–476.

[10] Xia, Z., Connington, K.W., Rapaka, S., Yue, P., Feng, J.J., and Chen, S. (2009) Flow patterns in the sedimentation of an elliptical particle. *Journal of Fluid Mechanics* **625**, 249–272.